(NASA-TM-79134) EFFECT OF STEADY-STATE PRESSURE DISTORTION ON FLOW CHARACTERISTICS ENTERING A TURBOFAN ENGINE (NASA) 34 p
HC A03/MF A01 CSCL 21E

N79-23969

Unclas
G3/07 22098

NASA Technical Memorandum 79134

AVRADCOM Technical Report 79-19

EFFECT OF STEADY-STATE PRESSURE DISTORTION ON FLOW CHARACTERISTICS ENTERING A TURBOFAN ENGINE

Ronald H. Soeder
Lewis Research Center

and

George A. Bobula
Propulsion Laboratory
AVRADCOM Research and Technology Laboratories
Lewis Research Center
Cleveland, Ohio

April 1979

SUMMARY

An investigation was conducted to determine the effect of steady-state circumferential pressure distortion on flow at the inlet of a turbofan engine. For this purpose flow angle, static-pressure, and total-pressure instrumentation was placed between a rotatable assembly and the engine inlet guide vanes. Five circumferential screen configurations and one circumferential solid-plate configuration were separately mounted on the assembly. For all of the configurations, measurements were recorded at each of thirty-six 10° steps of assembly rotation. Experiments were conducted with low-rotor speeds of 6000 and 8600 rpm and Reynolds Number Indices of 0.5, 0.35, and 0.2.

Near the engine inlet the circumferential variation of flow direction (yaw angle) was far greater than the radial variation (pitch angle). Yaw angle was usually largest at the hub and increased at tip, midspan and hub as flow approached the engine inlet. Change in engine speed only slightly affected yaw angle distribution, and variation of Reynolds Number Index had no effect.

Along the inlet-duct and extended bullet nose walls the magnitude of screen-generated static pressure increased exponentially as the flow approached the engine inlet. Wall static-pressure distortion was also a function of distortion harmonic. Freestream total pressure displayed no distortion variation with axial distance for any of the screen configurations employed in the investigation. The 60°-extent solid plate, however, generated circumferential pressure distortion that decreased as the flow approached the engine.

INTRODUCTION

Flow angle, static-pressure, and total-pressure distributions were measured in the passage between a turbofan engine inlet and upstream circumferential distortion screens. Although total-pressure and/or temperature distributions have been the principal elements in inlet distortion work, flow angle and static-pressure distributions are also important. Examples of this importance are modeling compressor interaction with flow distortion and selecting screens to produce specific flow patterns. Considerable flow redistribution occurs ahead of an engine with flow distortion. Immediately downstream of a circumferential screen total-pressure and velocity distortions are prevalent while static-pressure distortion is very small. The velocity distortion is attenuated as flow approaches an engine, and since there is no work on the fluid to change the total pressure, the static-

pressure distortion is correspondingly amplified. In reference 1 this velocity distortion attenuation and static-pressure distortion amplification were predicted to be exponential.

Recent analytical work includes a compressor model (refs. 2 and 3) that can calculate engine inlet distributions of velocity, static pressure and flow angle when the circumferential inlet total-pressure profile and compressor system operating conditions are given. Adequacy of model calculations was demonstrated by good agreement between predicted and measured flow angle for a 120°-extent distortion screen.

Past research programs at the Lewis Research Center have investigated some of these inlet flow distributions. These programs included engine tests with 180°-extent flow distortion (refs. 4 to 6) and transonic fan stage tests with 90°-extent distortion (ref. 7). All of these programs except one (ref. 5) measured static pressure along the inlet duct, and only the fan program measured inlet flow angle. Reference 3 also presented some Lewis Research Center static-pressure distortion data which supported the exponential amplification prediction of reference 1.

In this investigation these inlet distributions were examined for variations caused by changes of circumferential distortion, turbofan low-rotor speed (airflow), and inlet Reynolds Number Index. Freestream flow angles were measured in radial surveys at 2 axial locations including the engine inlet guide vanes, and static pressures were measured along the inlet duct and extended engine bullet nose walls. Circumferential profile resolution was increased by using a rotating distortion screen procedure similar to that of reference 6. Data was collected for corrected low-rotor speeds of 6000 and 8600 rpm and at Reynolds Number Indices of 0.2, 0.35, and 0.5.

APPARATUS

Engine

The engine used for this investigation was a production TF30-P-3 twin-spool turbofan engine. The engine has fixed inlet guide vanes (IGV's), 7th and 12th stage compressor bleeds, and a variable exhaust nozzle. The engine was installed in an altitude chamber by a direct-connect type of installation as shown in figure 1. An engine schematic and inlet instrumentation stations between the rotatable screen assembly and engine inlet guide vanes are shown in figure 2.

Distortion Device

Inlet pressure distortion was generated with a variety of circumferential screen configuration mounted on a motor driven rotatable screen assembly (fig. 3) located approximately one engine diameter or 0.951 m (37.4 in.) upstream of the engine inlet guide vanes. During these tests five different distortion screen configurations and one solid plate configuration were employed. Distortion screen descriptions are given in Table I.

As utilized in references 3 through 5 an extended bullet nose was installed between the distortion device and the engine inlet (fig. 2). This extended bullet nose provided the surface for the installation of a row of hub static taps and hub boundary layer yaw measurements.

Instrumentation

Inlet duct and engine face instrumentation between the distortion screen and inlet guide vanes is outlined diagrammatically in figures 2 and 4. Not all of the instrumentation in these figures was used to measure data presented in this report. (This investigation was only one segment of a five part test program.) Pressures were recorded on scanivalves and calibrated for a range of 0 to 69 kPa (10 psia).

The inlet duct and extended bullet nose wall boundary layer yaw (circumferential variation) probes are detailed in figure 5. Yaw angle is positive when the tangential flow component is in the direction of fan rotation. A positive yaw angle ($+\beta$) is noted in figure 5. An inlet guide vane pitch-yaw probe is sketched in figure 6. This probe is mounted on the leading edge of an inlet guide vane and measures the freestream pitch (radial variation) angle in addition to the yaw angle of a streamline. The sign convention for yaw angle is the same as for the boundary layer yaw measurements, and the pitch angle is positive when the radial flow component is oriented from tip to hub (fig. 6). The station 2 pitch-yaw probe is of similar design. Flow angle probes were circumferentially positioned at duct locations which avoided wakes from upstream instrumentation. Probe calibrations were obtained over a flow angle range of $\pm 30^{\circ}$ at the same stream Mach number conditions as encountered during engine tests. The estimated systematic error is about $\pm 2/3^{\circ}$, and the random error is roughly $\pm 1/2^{\circ}$. Additional information on flow angle measurements is found in reference 8.

Procedure

A motor-driven rotatable screen assembly containing a circumferential distortion screen or plate was rotated a full revolution in thirty-six 10° increments. After each screen assembly step and upon achieving steady-state engine operation, a data point was recorded. In most cases, presentation of a set of 36 data points starts with the distortion screen position beginning at 0° (see fig. 3) and the first data point plotted at its installed angular rake (or tap) position. The second data point was then plotted at a step of 10° but in the opposite direction to screen rotation. This procedure is analogous to holding the screen in the fixed position and rotating the instrumentation rakes. Pressure data was corrected to upstream plenum pressures in order to compensate for run-to-run variations.

At each of the inlet duct wall and bullet nose static taps (fig. 4), a maximum and minimum static pressure was identified for each test series of 36 data points. The difference between this maximum and minimum was normalized with a similar difference at the static taps nearest the IGV's (station 2B) and presented as a relative static distortion level.

The Reynolds Number Index (RNI) for each test run was held constant upstream of the distortion device by maintaining approximately a 289 K (520° R) inlet total temperature and adjusting the inlet total pressure to obtain the desired RNI value (0.5, 0.35, or 0.2).

RESULTS

Flow Angle

Clean inlet. - Figure 7 shows the undistorted streamline flow angles at the entrance to the inlet guide vanes (IGV's) as a function of corrected low-rotor speed. The pitch (radial variation) and yaw (circumferential variation) angles range between $+2^{\circ}$ and -2° and are relatively constant with changes in speed. The flow angle profiles presented in this report have not been corrected for the clean inlet configuration.

180° distortion. - Flow angles are presented in figures 8 to 11 for a 180°-extent, 49.4 percent blockage screen at a 8600 rpm corrected low-rotor speed and 0.5 Reynolds Number Index (RNI). The total-pressure distortion produced by the screen is 15.6 percent. The definition of total-pressure distortion plus distortion values for the other screen configurations are found in Table II.

The first observation is that at the IGV inlet, the pitch angle variation of a streamline as shown in figure 8 is much smaller than the yaw angle variation as

shown in figure 9 ($\pm 4^{\circ}$ compared to $\pm 15^{\circ}$). In addition, figure 8 shows that there is little difference in midspan and tip pitch angle magnitudes while the hub has a slightly larger variation. Consequently, the variation of pitch angle associated with the other screen configurations will not be presented.

Figures 9 to 11 show that the circumferential variation of yaw angle is also largest in the hub region. Although yaw angle increases as flow approaches the IGV inlet (sta. 2C), the hub to tip differences are less at station 2C than they are at station 2. This increase in yaw angle is caused by engine pumping effects and corresponding distorted flow redistribution. The station 2 boundary layer yaw data in figure 11 was obtained with the outer most immersion probes.

The maximum and minimum yaw angles are not at the edges of the distortion screen but are within the distorted sector of the flow field. This indicates that the extent of the low pressure field is slightly less than the intended 180°. Also at these edge points a yaw angle measurement error of approximately 1° occurs because of the steep total-pressure gradients. This error is in addition to that mentioned in the Instrumentation section. A correction would decrease the yaw angle magnitude at these locations.

Reynolds Number and speed effects with distortion. - RNI effects on streamline yaw angles at the IGV's (sta. 2C) are presented in figure 12. A 180°-extent, 34.6 percent blockage screen was used at a corrected low-rotor speed of 8600 rpm. No influence on streamline yaw angle is observed as the RNI changes from 0.5 to 0.35. Boundary-layer and freestream streamline yaw angles at station 2 (no figure included) also showed no variation in yaw angle with RNI. As in previous figures the largest yaw angle variation occurs in the hub region of the engine inlet.

Corrected speed (airflow) effects on station 2C streamline yaw angle is shown in figure 13 for the 49.4 percent blockage screen. It is observed that a decrease in low-rotor speed from 8600 to 6000 rpm resulted in a slight lowering of the yaw angle curve in the distorted flow region.

Screen blockage and extent effects. - The data in figure 14 shows that the magnitude of streamline yaw angle at entrance to the IGV's decreases as screen blockage is reduced. The variation of RNI values as indicated in the figure can be discounted based on the previous section's discussion.

Figure 15 presents engine inlet circumferential variation of maximum yaw angle measurements for the 180° graded screen distortion (hub), the 2-per-rev 120° distortion (tip) and the 60° solid plate distortion (tip). For all three patterns, the lowering of the data curves in the distortion screen region with speed reduction is

evident. Also, as discussed previously, figure 15(b) shows a reduction in distortion extent from the original screen pattern.

Figure 16 compares the graded screen distortion pattern with the 180°-extent, 34.6 percent blockage screen. The maximum yaw angle change and the undistorted flow region profile are almost identical for both screens, yet the graded screen produces a greater total-pressure distortion (12.9% versus 10.2%) and has less of a yaw angle variation at the screen edges. Such a screen might be useful when structural loading on blades is a consideration during engine testing with flow distortion.

Static-Pressure Distortion

Figures 17 through 21 investigate the static-pressure distortion change along the inlet duct wall and bullet nose extension for variations in low-rotor speed, RNI, screen blockage, distortion harmonic, and screen extent. The static-pressure distortion was obtained by determining the maximum and minimum pressures at each static tap location from the test set of 36 data points (see Procedure). The distortion change presented in this report is similar to that used in reference 3 and is defined as $(P_{S,\,max} - P_{S,\,min})$ for each location normalized by $(P_{S,\,max} - P_{S,\,min})$ at station 2B or $\Delta P_S/(\Delta P_S)2B$.

Except for the solid plate tests, these figures show that the exponential curve of reference 1 satisfactorily predicts the static-pressure distortion amplification immediately in front of the engine. At distances greater than one mean radius (r_m) ahead of the engine, the exponential curve lies below the measured data. Flow in this region of x/r_m greater than 1 is more complex than the simple flow model used to derive the exponential prediction. The disruptive effects of rake blockage at station 2A is also prominent. The following discussion is therefore confined to the region between the engine inlet and station 2A (x/r_m values less than 1.0).

Figure 17 shows the bullet nose data to be slightly closer to the exponential prediction than the duct wall points. From the bullet nose data of figures 17 to 20 one sees that the influence of rotor speed, screen blockage, and patterns shape (graded versus uniform) is small whereas a possible RNI effect may exist. Figure 20 shows the 120°-extent, 2-per-rev screen data to be in good agreement with a second harmonic (n equals 2) exponential prediction based on reference 1. The first harmonic (n equals 1) was used for the other figures.

Figure 21 shows the variation of static-pressure data along the inlet duct wall and extended bullet nose for tests using a 60°-extent solid plate. The data does not follow the exponential curve because the flow downstream of the plate is a three-

dimensional flow field with eddy currents in the low pressure region. Such a flow field is too complex for prediction by reference 1.

Pressure Profiles

Figure 22 describes the axial variation of freestream rake-average total pressures from station A (downstream of the screen) to station 2C (IGV entrance) and the axial variation of duct wall static pressures from station A to station 2B (6.17 cm upstream of the IGV's inlet).

The total-pressure profiles show that there is no change in total-pressure level with axial distance. The total-pressure profile at the edges of the screen indicates a low-pressure field contraction as the airflow approaches the IGV's (dashed line to solid line). This supports the previous observation that the maximum and minimum yaw angles occur within the distortion screen sector of the flow field instead of at the screen edges (figs. 9 and 15).

Figure 22(b) shows that the static-pressure profile increases from nearly a constant level at station A to sinusoidal at station 2B. The amplitude increase with axial distance would be exponential as discussed in the Static-Pressure Distortion section.

Figure 23 shows the pressure level decrease of the 6000 rpm data as compared to 8600 rpm data of figure 22. Again the total-pressure levels are unchanged with axial distance.

Figure 24 shows that there is no RNI effect on the total or static-pressure profiles at the inlet to the IGV's. The solid line in figure 24(b) shows a predicted static-pressure profile using Mazzawy's model (ref. 3). Although the model prediction is for the IGV inlet, it is compared to station 2B data (static measurements are not available at the IGV inlet). Note that while the pressure levels are satisfactorily predicted, the model was unable to match the sinusoidal profile.

Figure 25 shows the variation in total-pressure profiles produced by screens and a solid plate of different extents. Data obtained with the graded screen, figure 25(a) and the two screens of 120°-extent, figure 25(b), show that no axial variation in total-pressure profile occurs between station A and station 2C for the same conditions of low-rotor speed (airflow) and RNI. Figure 25(c) shows that the total-pressure amplitude behind the plate attenuates as flow approaches the IGV's.

SUMMARY OF RESULTS

A TF30-P-3 turbofan engine fitted with an extended bullet nose was tested with inlet circumferential pressure distortion. The results of inlet flow angle, static-pressure distortion, and circumferential pressure profile measurements are summarized as follows:

1. Pitch angle (radial variation) is much smaller than yaw angle (circumferential variation).

2. Yaw angle variation is usually largest in the hub region for the screen configurations tested. Yaw angle variation increases in magnitude as flow approaches the engine inlet.

3. RNI variations 0.5 and 0.35 have a negligible effect on yaw angle.

4. Low-rotor speed (airflow) variations of 8600 and 6000 rpm have a slight effect on yaw angle in the low-pressure region of the flow.

5. Increasing the screen blockage increases the yaw angle variation.

6. A graded screen pattern with the same yaw angle variation magnitude as a uniform screen pattern produces a larger total-pressure distortion.

7. Screen-induced static-pressure distortion increases exponentially as flow approaches the engine and is a function of the distortion harmonic.

8. Screen-induced total-pressure circumferential profiles remain nearly constant as flow approaches the engine. The percent total-pressure distortion does not change with RNI variation.

9. The solid-plate induced total-pressure distortion decreases as flow approaches the engine.

APPENDIX A

SYMBOLS

e	natural Logarithm base
IGV	inlet guide vane
N1	low-rotor speed, rpm
N1R2	low-rotor speed corrected to station 2 test conditions, $N1/\sqrt{\theta_2}$, rpm
n	Fourier harmonic integer; 1, 2, 3
P	pressure, Pa
RNI	Reynolds Number Index, $\delta/(\mu/\mu_{SLS}) \cdot \sqrt{\theta}$
r_m	mean radius of IGV, 0.34 m
T	temperature, K
U	tangential velocity, m/sec
V_a	axial velocity, m/sec
x	axial length, m
Δ	maximum-minimum value
α	pitch angle, deg
β	yaw angle, deg
δ	ratio of total pressure to standard sea-level static pressure
θ	ratio of total temperature to standard sea level static-temperature
μ	absolute viscosity, kg/(m-sec)

Subscripts:

A	station A, pressure measurement station located 83.55 cm upstream of inlet guide vanes
AVG	average
B	station B, row of static taps along inlet duct wall and extended bullet nose
max	maximum
min	minimum
S	static condition

SLS	standard sea-level static condition
T	total condition
1	station 1, airflow metering station, located 250.24 cm upstream of inlet guide vanes
2	station 2, engine inlet temperature and flow angle measurement, located 13.39 cm upstream of the inlet guide vanes
2A	station 2A, engine inlet pressure measurement, located 44.41 cm upstream of the inlet guide vanes
2B	station 2B, start of static pressure taps along the inlet duct wall and extended bullet nose, located 6.17 cm upstream of the inlet guide vanes
2C	station 2C, flow angle measurement at entrance to inlet guide vanes

REFERENCES

1. Plourde, G. A.; and Stenning, A. H.: Attenuation of Circumferential Inlet Distortion in Multistage Axial Compressors. J. Aircraft, vol. 5, no. 3, May-June 1968, pp. 236-242.

2. Mazzawy, R. S.: Multiple Segment Parallel Compressor Model for Circumferential Flow Distortion. J. Eng. Power, vol. 99, no. 2, Apr. 1977, pp. 288-296.

3. Mazzawy, R. S.; and Banks, G. A.: Modeling and Analysis of the TF30-P-3 Compressor System with Inlet Pressure Distortion. (PWA-5302, Pratt and Whitney Aircraft; NASA Contract NAS3-18535.) NASA CR-134996, 1976.

4. Evans, D. G.; et al.: Some Comparisons of the Flow Characteristics of a Turbofan Compressor System with and without Inlet Pressure Distortion. NASA TM X-71574, 1974.

5. de Bogdan, C. E.; et al.: Effect of a 180° Extent Inlet Pressure Distortion on the Internal Flow Conditions of a TF30-P-3 Engine. NASA TM X-3267, 1975.

6. de Bogdan, C. E.; Moss, J. E., Jr.; and Braithwaite, W. M.: Internal Flow Characteristics of a Multistage Compressor with Inlet Pressure Distortion. NASA TM X-3446, 1977.

7. Sanger, N. L.: Performance of a 1.57-Pressure-Ratio Transonic Fan Stage with a Screen-Induced 90° Circumferential Inlet Flow Distortion. NASA TN D-8163, 1976.

8. Dudzinski, T. J.; and Krause, L. N.: Flow-Direction Measurement with Fixed-Position Probes. NASA TM X-1904, 1969.

TABLE I. - SCREEN REQUIREMENTS

Screen no.	Wire diameter, cm (in.)	Width of opening, cm (in.)	Blockage, percent	Extent, deg
1	0.081 (0.032)	0.201 (0.079)	49.4	180
2	0.089 (0.035)	0.373 (0.147)	34.6	180
3	0.089 (0.035)	0.546 (0.215)	26	180
4 (Graded screen)	0.089 (0.035)	0.373 (0.147)	34.6	60
	0.119 (0.047)	1.151 (0.453)	17.9	120
	0.089 (0.035)	0.546 (0.215)	26	180
5	0.183 (0.072)	0.325 (0.128)	59	120- 2 sectors
6	------	------	100	60

TABLE II. - SCREEN TOTAL-PRESSURE DISTORTION

Screen no.	Test conditions		$\left(\frac{P_{T,\,max} - P_{T,\,min}}{P_{T,\,AVG}}\right)$, percent (a)
	N1R2, rpm	RNI_1	
1	6000	0.50	6.1
	8600		15.6
2	8600	0.50	10.2
		0.35	
3	8600	0.20	7.0
4 (Graded screen)	6000	0.50	5.4
	8600		12.9
5	6000	0.50	9.7
	8600		27.5
6	6000	0.50	16.2
	8600		30.6

(a) $P_{T,\,max}$ and $P_{T,\,min}$ are maximum and minimum rake average total pressures at stations 2 and 2A.

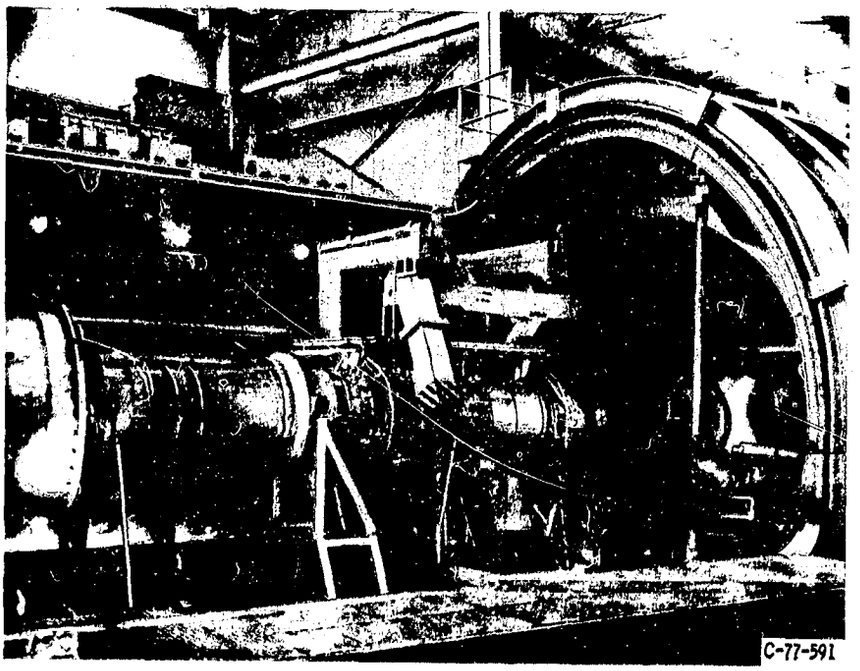

Figure 1. - TF-30-P-3 engine in altitude test chamber.

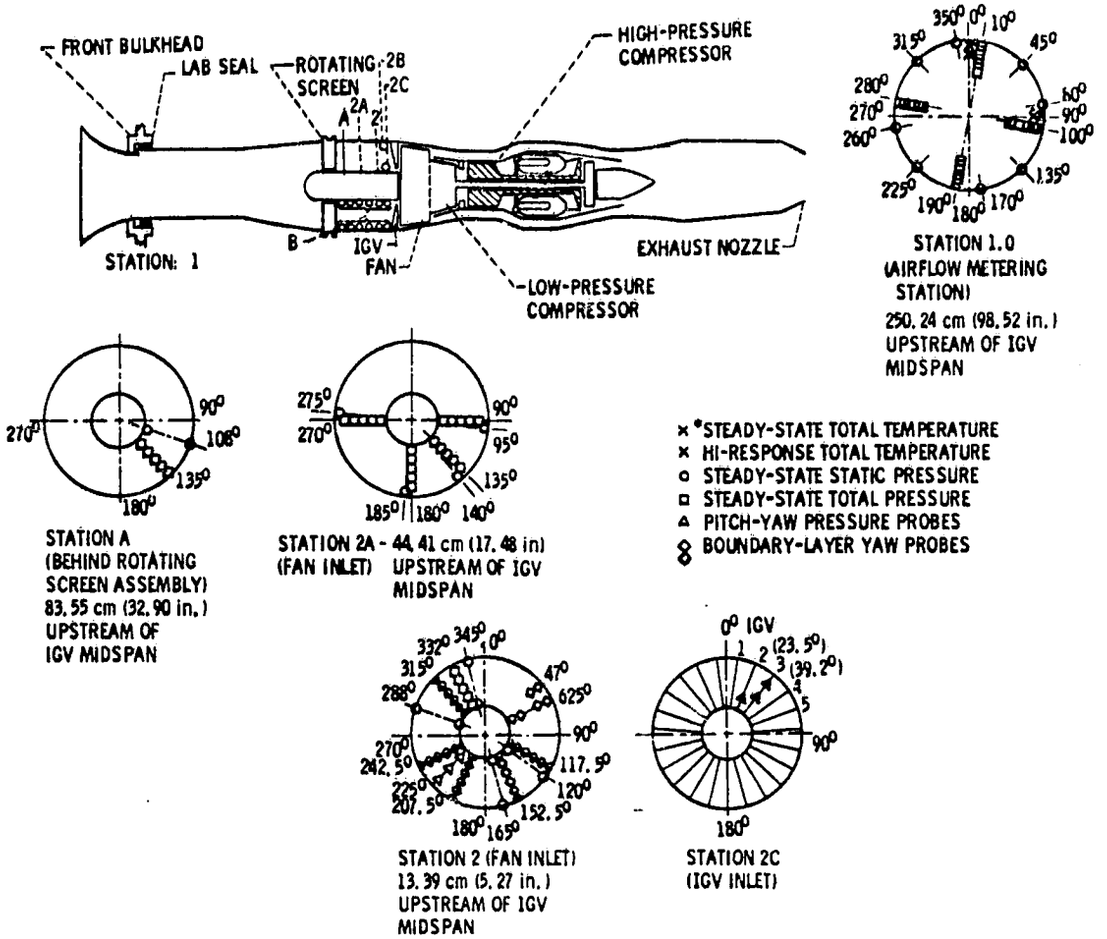

Figure 2. - Instrumentation layout for TF30-P-3 turbofan engine. (Instrumentation stations viewed looking upstream.)

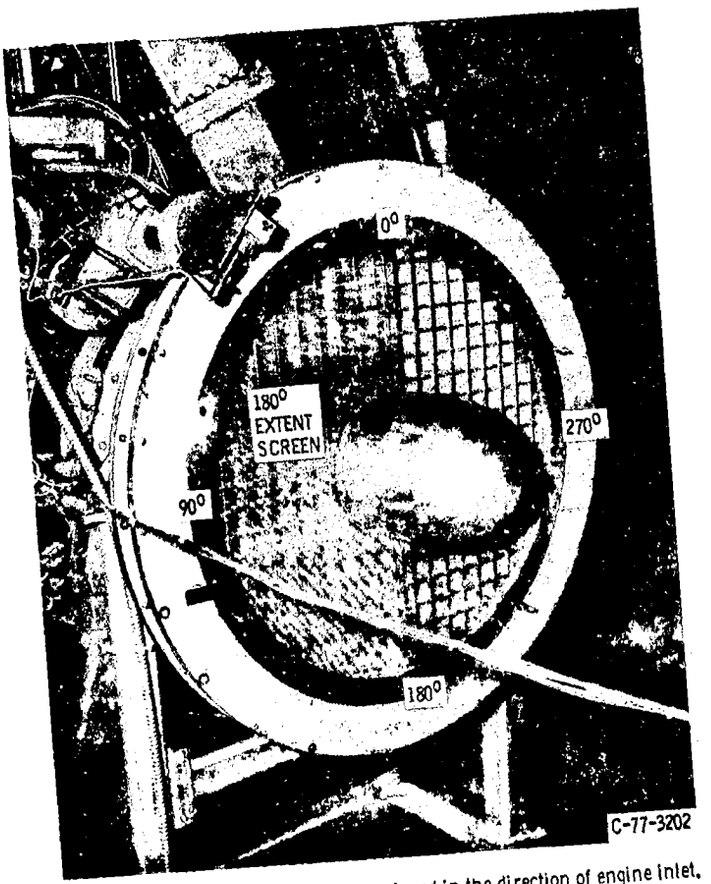

Figure 3. - Rotating screen assembly, viewed in the direction of engine inlet.

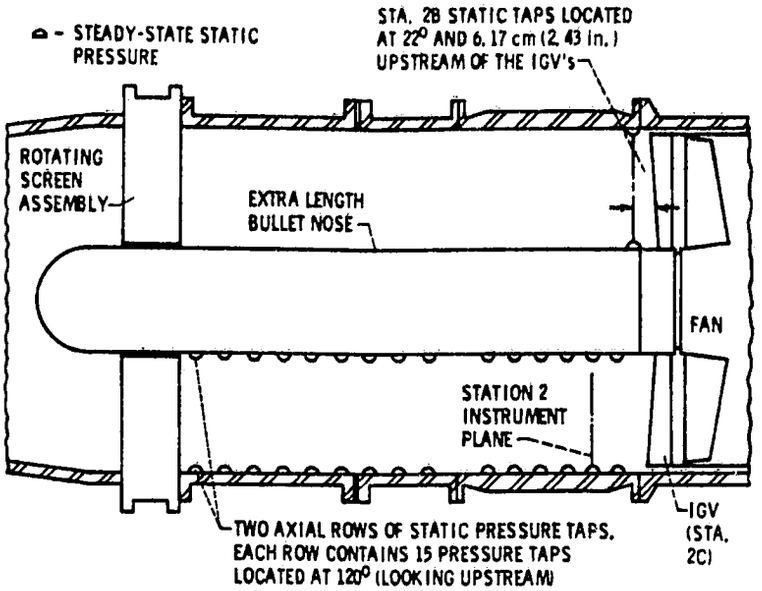

Figure 4. - Bullet nose extension, Station B.

PROBE	D	E	NO. REQUIRED
TIP	0.51 cm (0.20 in.)	1.02 cm (0.40 in.)	2
HUB	0.38 cm (0.15 in.)	0.64 cm (0.25 in.)	1

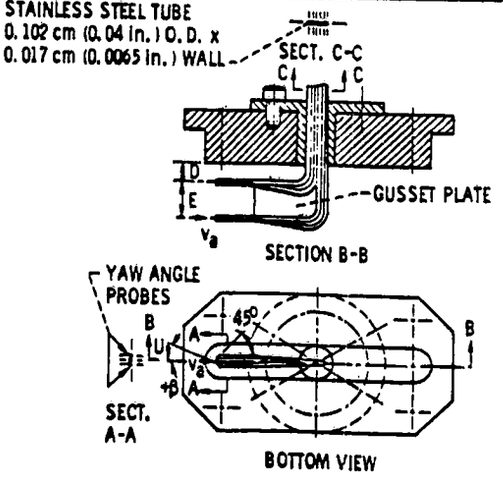

Figure 5. - Tip and hub boundary layer yaw probes located at Station 2 and at 5.1 cm (2 in.) upstream of Station 2.

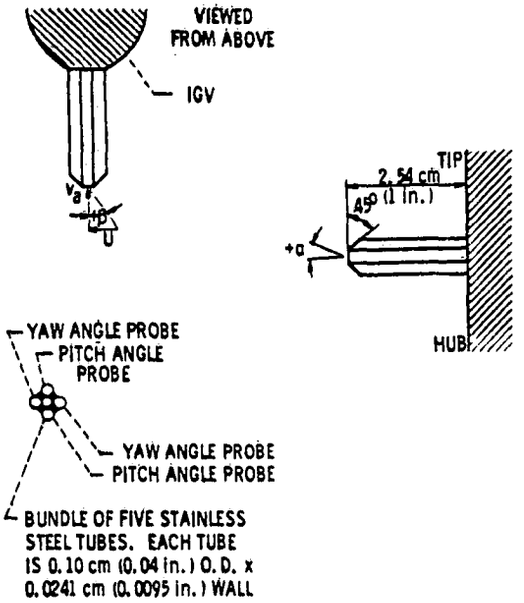

Figure 6. - Sketch of pitch-yaw pressure measurement probes located at station 2C.

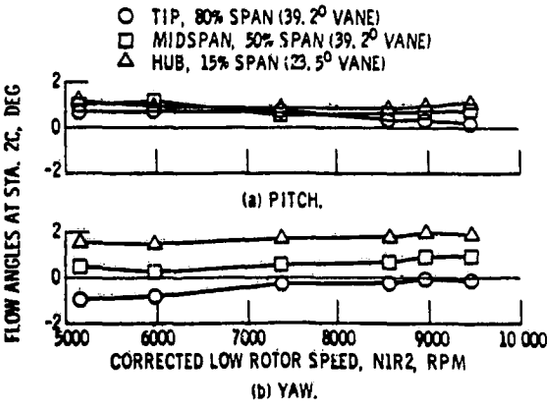

Figure 7. - Flow angles at Sta. 2C (inlet to IGV's) versus low-rotor speed with no pressure distortion (clean inlet), 0.5 RNI.

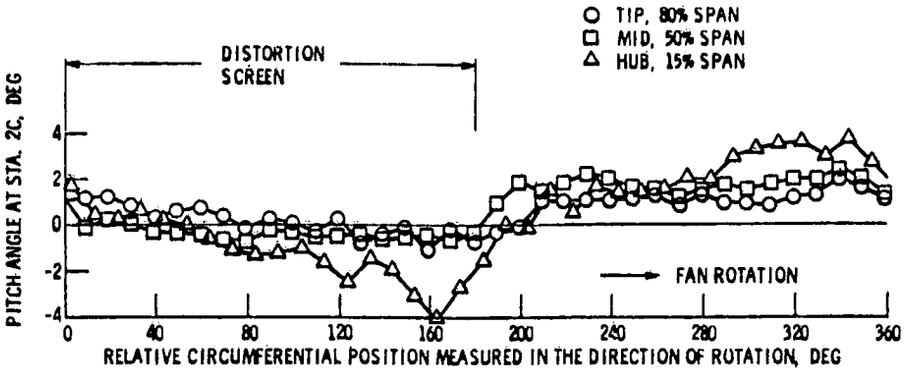

Figure 8. - Pitch angle variation at Sta. 2C for 180°-extent, 49.4 percent blockage screen. 8600 rpm corrected low-rotor speed and 0.5 RNI.

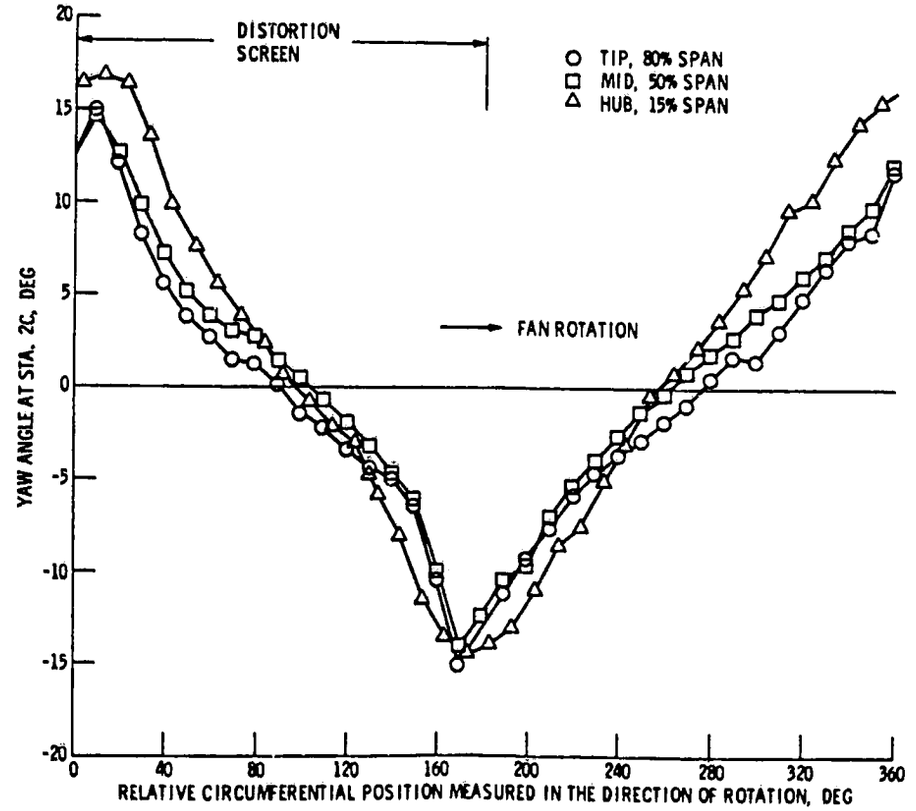

Figure 9. - Yaw angle variation at Sta. 2C for 180°-extent, 49.4 percent blockage screen. 8600 rpm corrected low-rotor speed and 0.5 RNI.

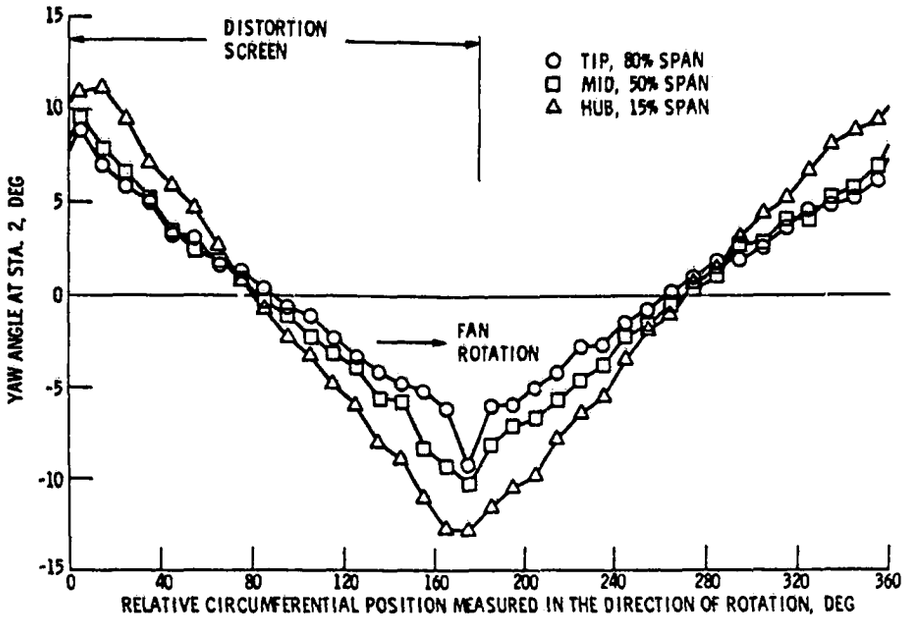

Figure 10. - Yaw angle variation at Sta. 2 for 180°-extent, 49.4 percent blockage screen. 8600 rpm corrected low-rotor speed and 0.5 RNI.

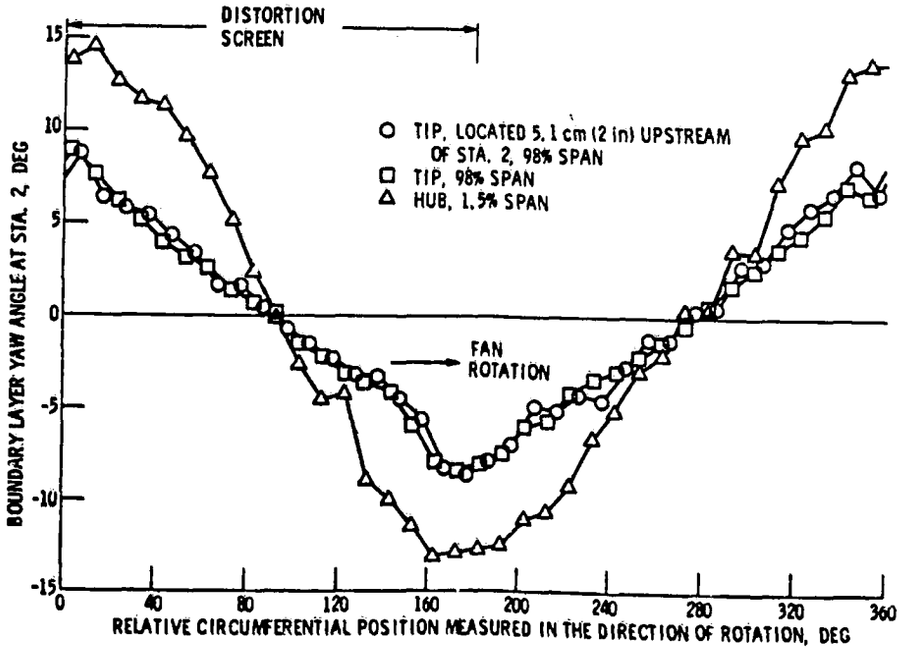

Figure 11. - Boundary layer yaw angle variation at Sta. 2 for 180°-extent, 49.4 percent blockage screen. 8600 rpm corrected low-rotor speed and 0.50 RNI.

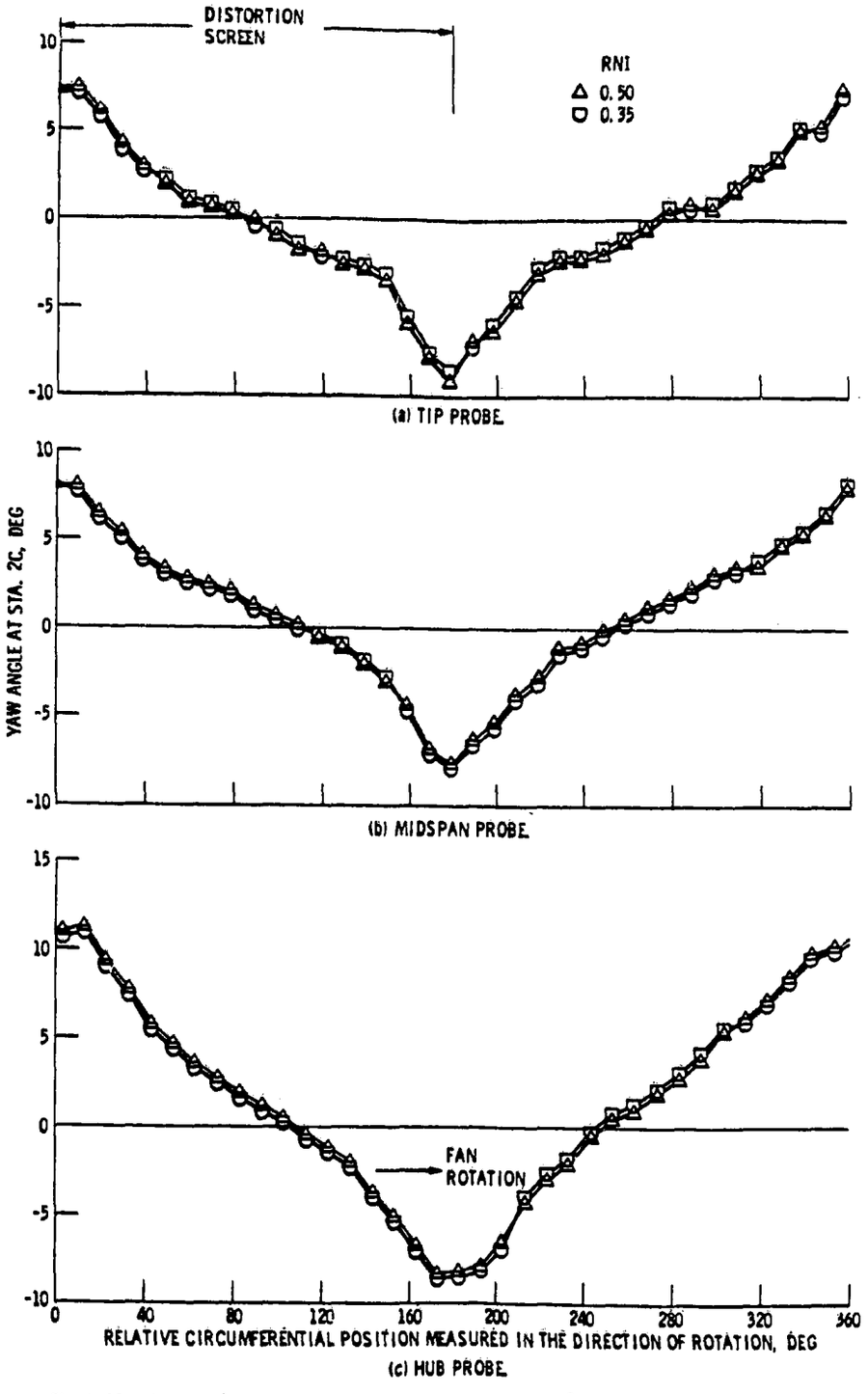

Figure 12. - Effect of RNI on yaw angle variation at Sta. 2C for 180°-extent, 34.6 percent blockage screen. 8600 rpm corrected low-rotor speed.

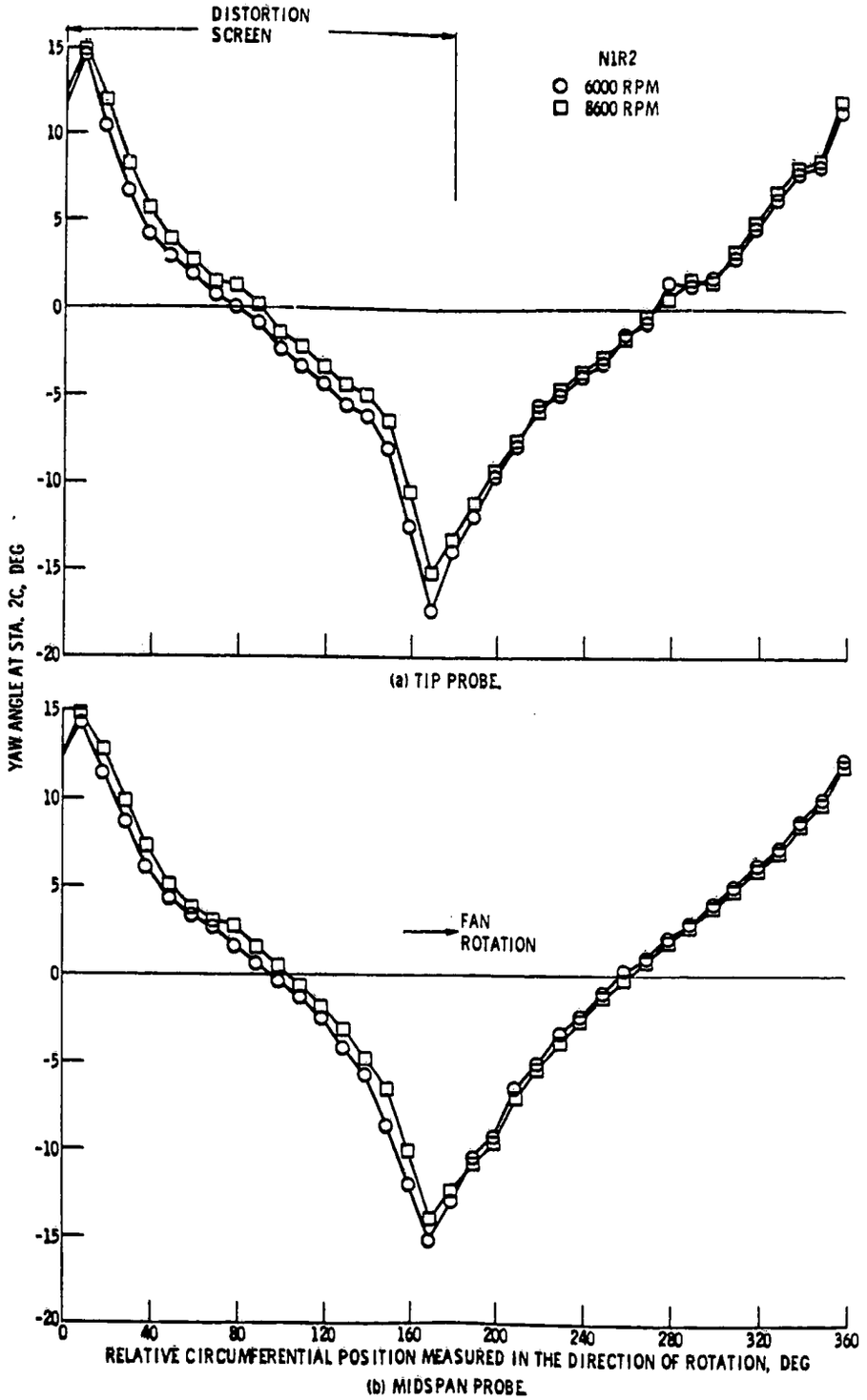

Figure 13. - Effect of corrected low-rotor speed on yaw angle variation at Sta. 2C for 180°-extent, 49.4 percent blockage screen, 0.50 RNI.

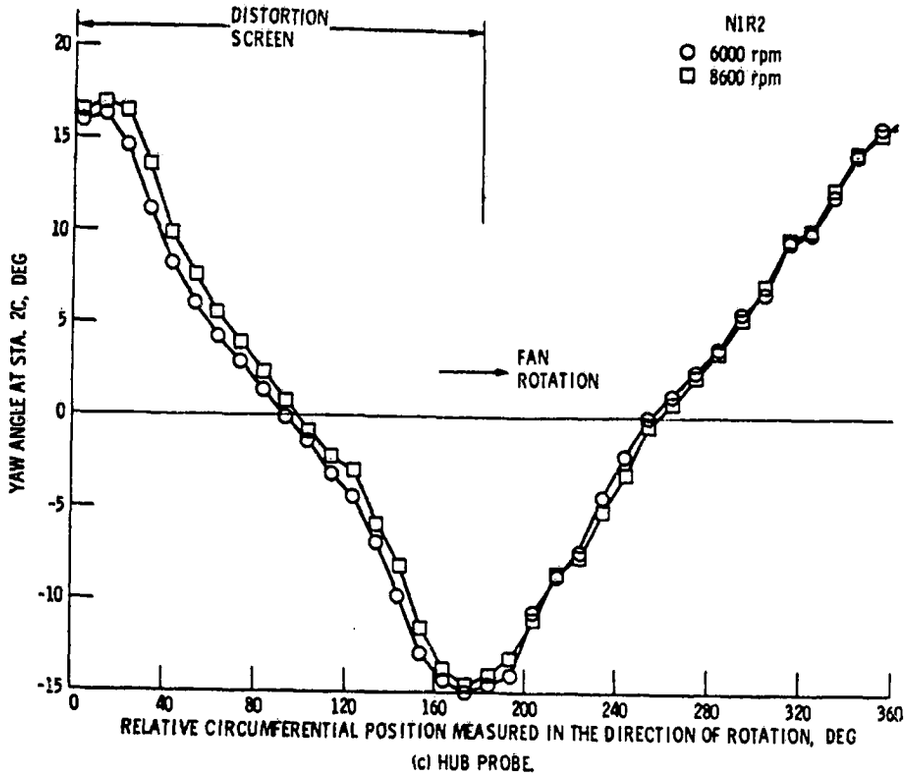

(c) HUB PROBE.

Figure 13. - Concluded.

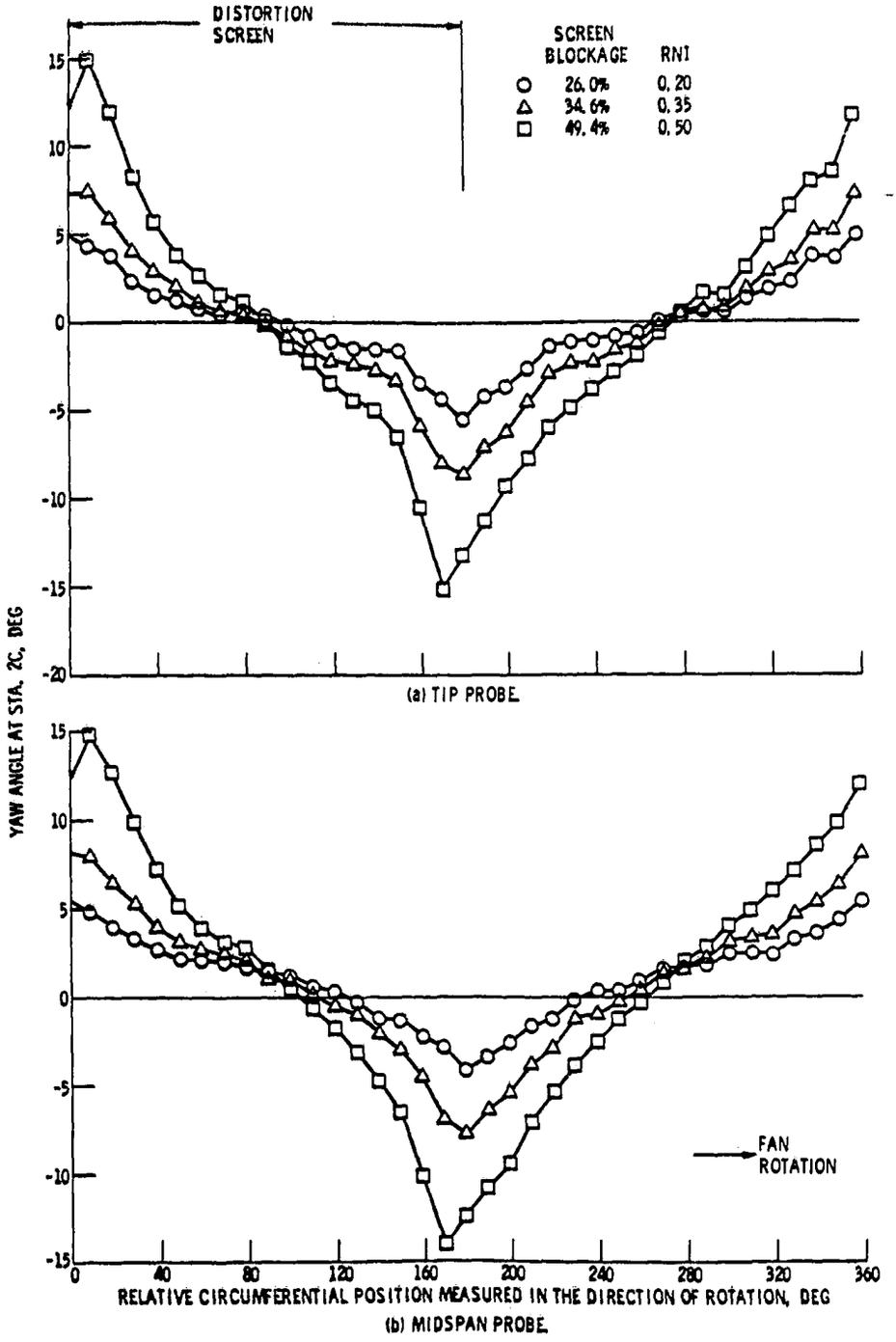

Figure 14. - Comparison of three screen blockages of 180°-extent on yaw angle variation at Sta. 2C. 8600 rpm corrected low-rotor speed.

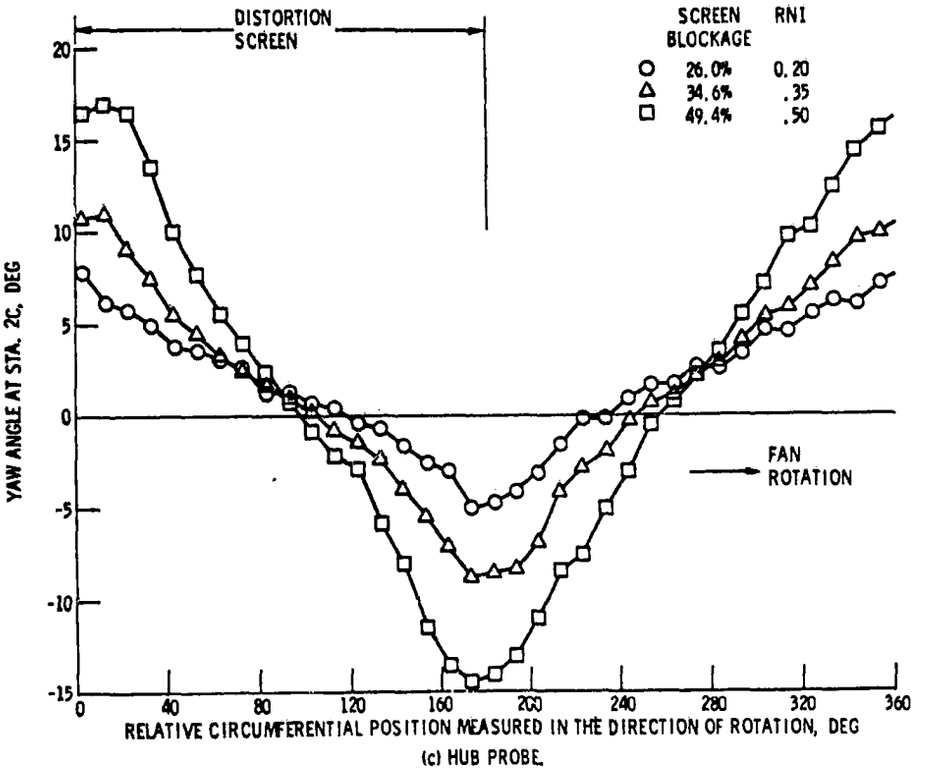

(c) HUB PROBE.

Figure 14. - Concluded.

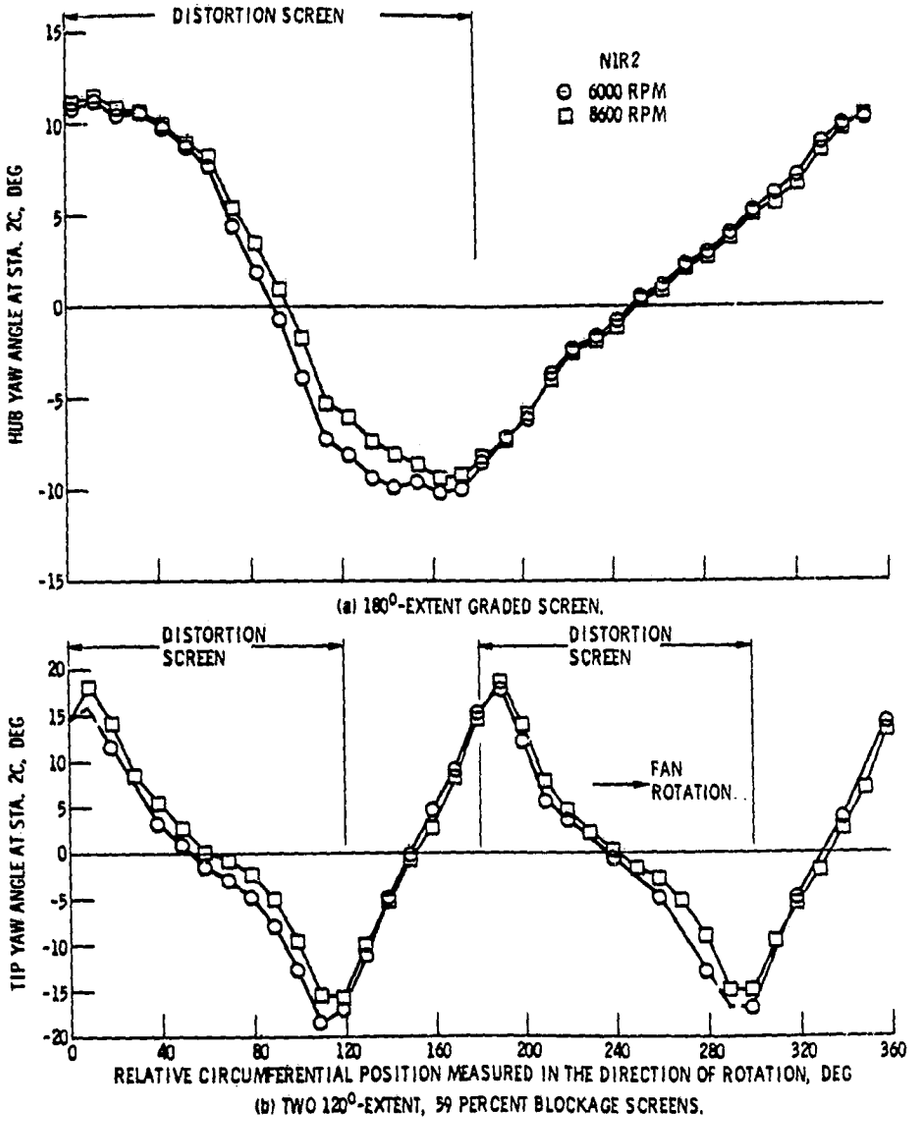

Figure 15. - Maximum (hub or tip) circumferential yaw angle variation at Sta. 2C for 180°-extent graded screen, 2-per-rev 120°-extent screens, and 60°-extent solid plate, 0.5 RNI.

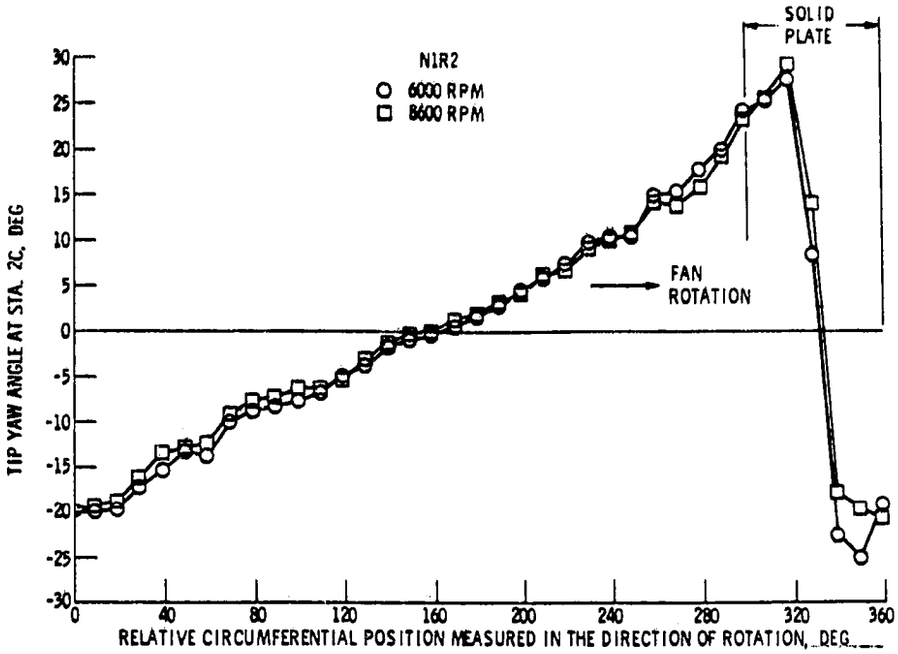

(c) 60°-EXTENT SOLID PLATE.

Figure 15. - Concluded.

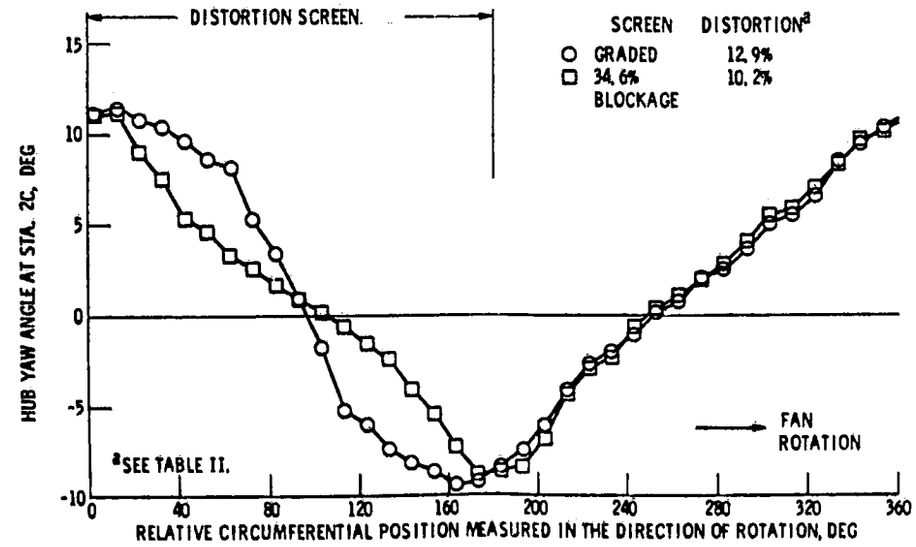

Figure 16. - Comparison of graded and uniform 180°-extent distortions on hub yaw angle variation at Sta. 2C. 8600 rpm corrected low-rotor speed and 0.5 RNI.

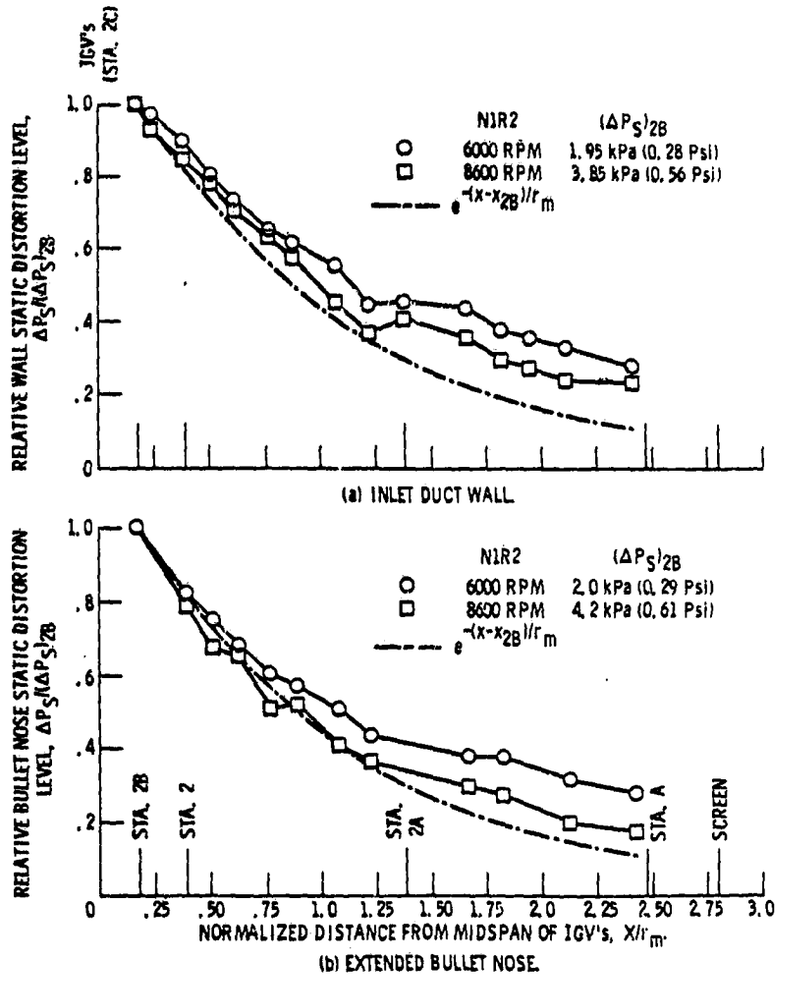

Figure 17. - Effect of corrected low-rotor speed on static-pressure distortion for 180°-extent, 49.4 percent blockage screen, 0.5 RNI.

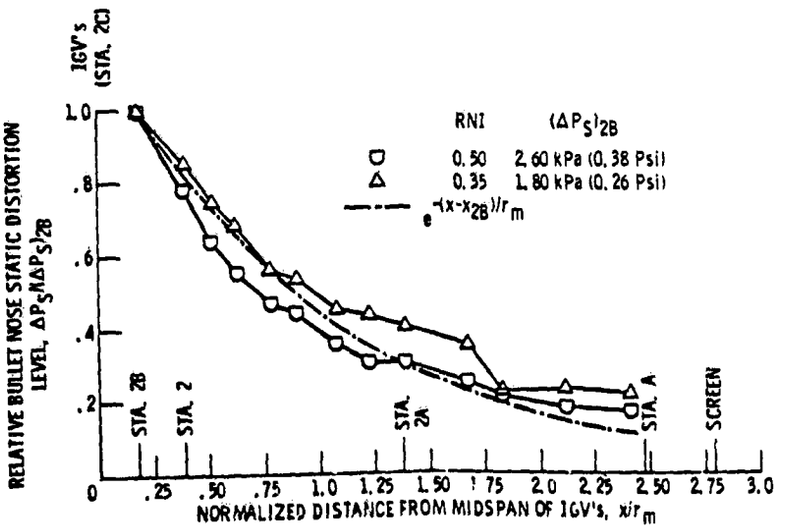

Figure 18. - Effect of RNI on static-pressure distortion along the extended bullet nose for 180°-extent, 34.6 percent blockage screen. 8600 rpm corrected low-rotor speed.

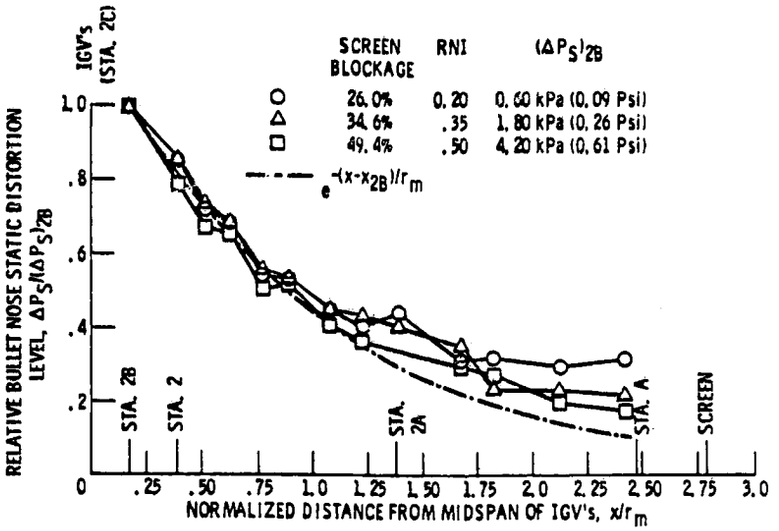

Figure 19. - Comparison of three screen blockages of 180°-extent on static pressure distortion along the extended bullet nose. 8600 rpm corrected low-rotor speed.

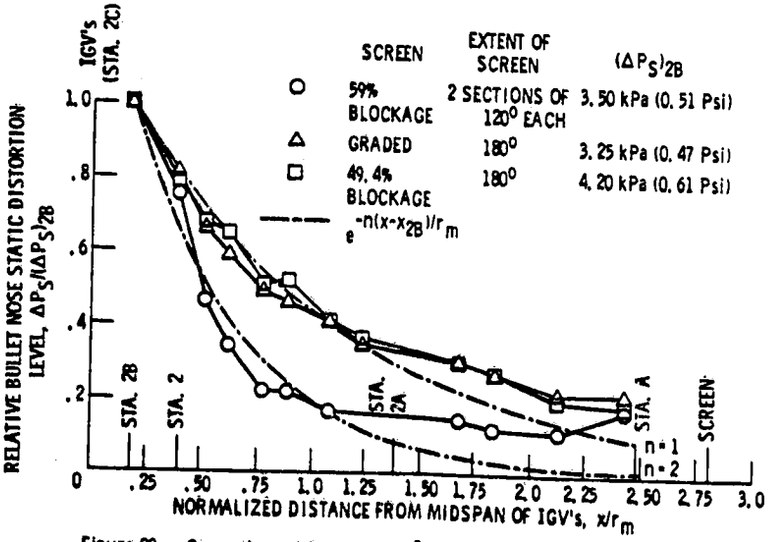

Figure 20. - Comparison of 2-per-rev 120°-extent screen, 180°-extent graded screen, and 180°-extent, 49.4 percent blockage screen. 8600 rpm corrected low-rotor speed and 0.5 RNI.

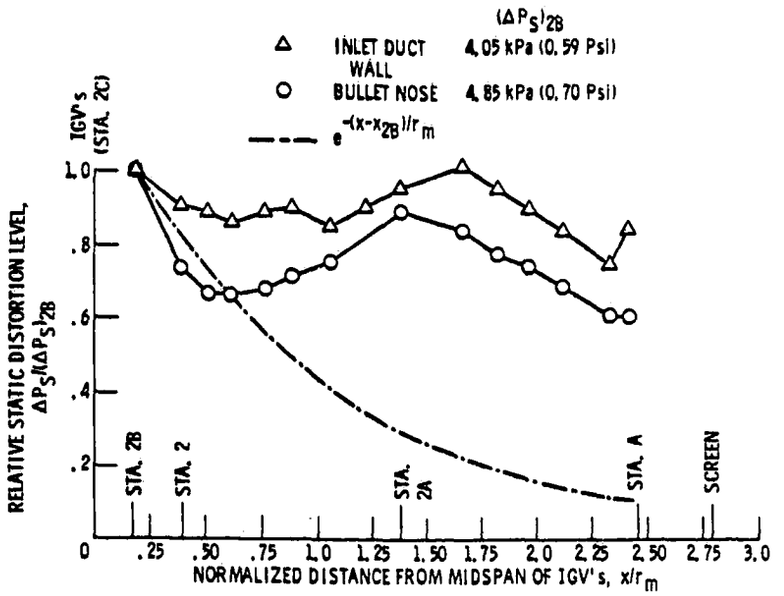

Figure 21. - Static pressure distortion for a 60°-extent solid plate. 8600 rpm corrected low-rotor speed and 0.5 RNI.

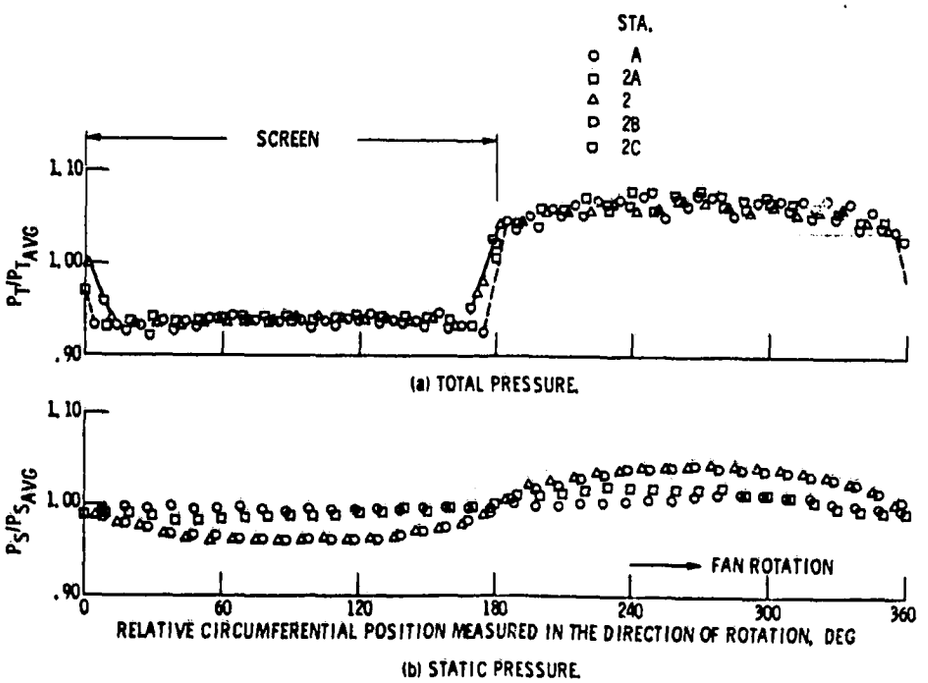

Figure 22. - Circumferential variation of total and static pressure for 180°-extent, 49.4 percent blockage screen. 8600 rpm corrected low-rotor speed and 0.5 RNI.

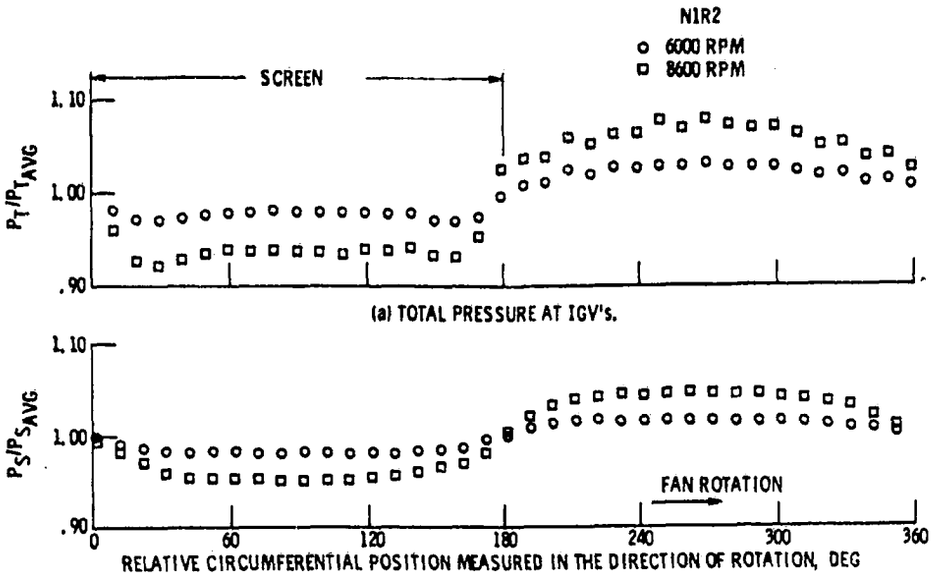

Figure 23. - Effect of corrected low-rotor speed on circumferential total and static-pressure variation for 180°-extent, 49.4 percent blockage screen and 0.5 RNI.

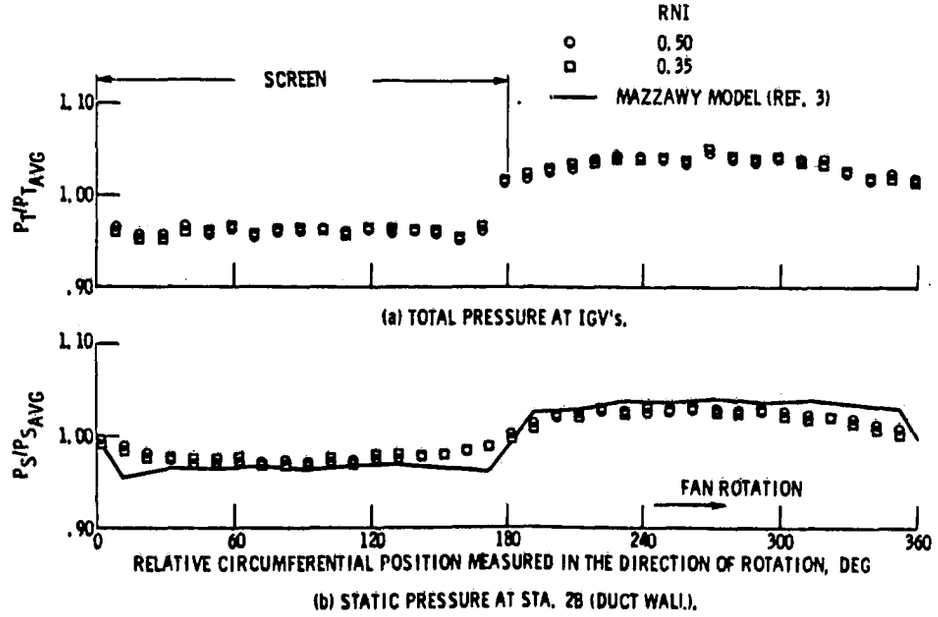

Figure 24. - Effect of RNI on circumferential variation of total and static pressure for a 180°-extent, 34.6 percent blockage screen. 8600 rpm corrected low-rotor speed.

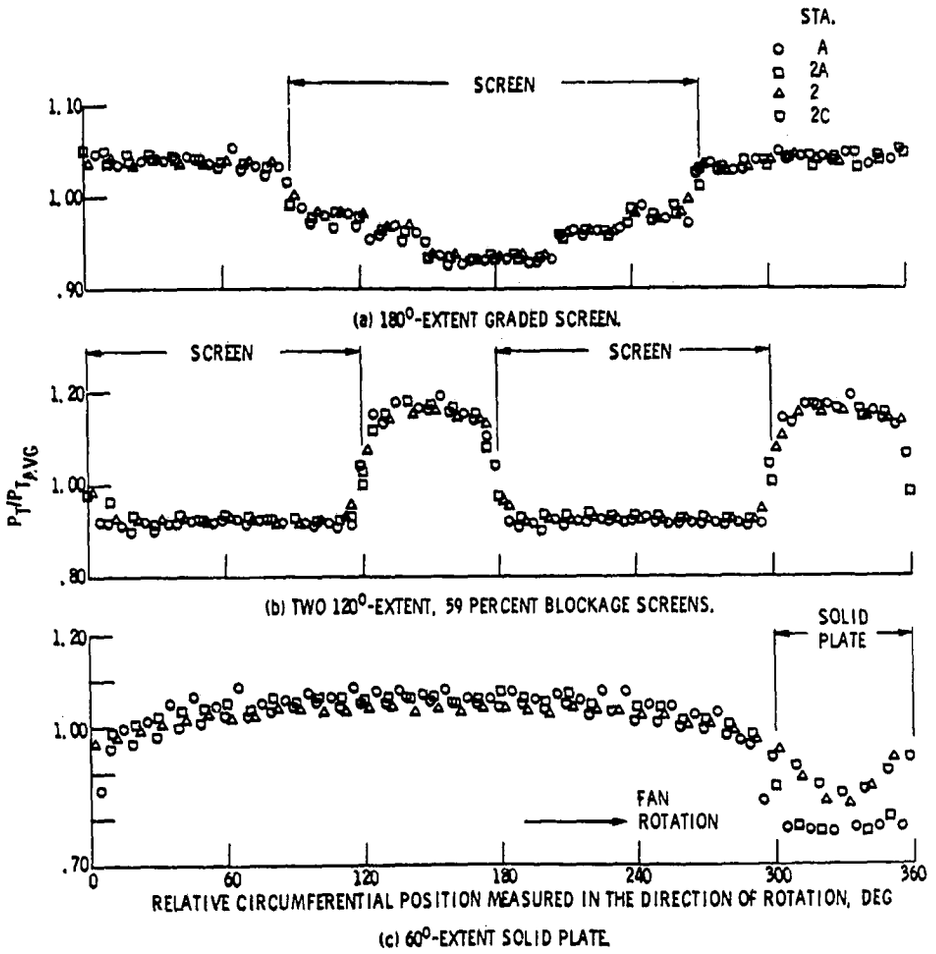

Figure 25. - Circumferential total-pressure variation for 180°-extent graded screen, 2-per-rev 120°-extent screens, and 60°-extent solid plate. 8600 rpm corrected low-rotor speed and 0.5 RNI.

1. Report No NASA TM-79134 AVRADCOM TR 79-19	2. Government Accession No.	3. Recipient's Catalog No
4. Title and Subtitle EFFECT OF STEADY-STATE PRESSURE DISTORTION ON FLOW CHARACTERISTICS ENTERING A TURBOFAN ENGINE		5. Report Date April 1979 6. Performing Organization Code
7. Author(s) Ronald H. Soeder and George A. Fiduccia		8. Performing Organization Report No. E-9982 10. Work Unit No.
9. Performing Organization Name and Address NASA Lewis Research Center and AVRADCOM Research and Technology Laboratories Cleveland, Ohio 44135		11. Contract or Grant No. 13. Type of Report and Period Covered Technical Memorandum
12. Sponsoring Agency Name and Address National Aeronautics and Space Administration Washington, D.C. 20546 and U.S. Army Aviation Research and Development Command, St. Louis, Mo. 63166		14. Sponsoring Agency Code

15. Supplementary Notes

16. Abstract

Flow angle, static-pressure, and total-pressure distributions were measured in the passage ahead of a turbofan engine operating with inlet pressure distortion. Distortions were generated with five screen configurations and one solid plate configuration. The screens and solid plate were circumferential and mounted on a rotatable assembly. Reynolds Number Index upstream of the distortion device was maintained at 0.5, 0.35, or 0.2, and engine corrected low-rotor speeds were held at 6000 rpm and 8600 rpm. Near the engine inlet, flow angle was largest at the hub and increased as flow approached the engine. The magnitude of static-pressure distortion measured along the inlet-duct and extended bullet nose walls increased exponentially as the flow approached the engine. Wall static-pressure distortion was also a function of distortion harmonic.

17. Key Words (Suggested by Author(s)) Turbofan engine Inlet flow angle Inlet static-pressure distortion Inlet total-pressure distortion	18. Distribution Statement Unclassified - unlimited STAR Category 07		
19. Security Classif. (of this report) Unclassified	20. Security Classif. (of this page) Unclassified	21. No. of Pages	22. Price*

* For sale by the National Technical Information Service, Springfield Virginia 22161